4 EXPERIMENTAL FACILITIES IN BEAM HALL

4.1 GENERAL PURPOSE SCATTERING CHAMBER AND NATIONAL ARRAY OF NEUTRON DETECTORS

N. Saneesh, K.S. Golda, Mohit Kumar, A. Jhingan and P. Sugathan

4.1.1 Experiments using GPSC and NAND facilities

National Array of Neutron Detectors (NAND) consisting of 100 liquid scintillators were used in experiments to study heavy ion-induced fusion-fission dynamics. A series of experiments were scheduled during the Pelletron-LINAC campaign last year. However, scheduled experiments were discontinued due to COVID-19 lock-down in the month of March 2020. During January-March 2020, four experiments were completed on mass gated neutron multiplicities and fission fragment mass distributions. ^{48}Ti and ^{28}Si beams, accelerated by the combination of Pelletron and LINAC, were used in these experiments. Neutrons were detected by the array of neutron detectors, in coincidence with fission fragments detected in a pair of multi-wire proportional counters (MWPC). The data were collected by a new VME-based data acquisition system in which events were stored in ROOT format. Detailed analysis of the data is being performed by users at various universities. Once the Pelletron accelerator operation was resumed after the lock-down, a limited number of user experiments were performed in the General Purpose Scattering Chamber (GPSC). These experiments covered fission fragment mass distribution, quasi-elastic scattering studies around barrier energies and incomplete fusion studies. Apart from these experiments, GPSC facility was used for regular experiments in the field of materials science and irradiation of micro-electronic devices by the scientists of the Indian Space Research Organization (ISRO).

Following experiments were performed in GPSC and NAND beamlines in the last academic year.

Table 4.1.1: List of experiments carried out in the academic year 2020-21.

User and Affiliation	Experiment
Mr. Rakesh Kumar, Kurukshetra University	Study of the dynamics of heavy ion induced fusion-fission reactions using ^{28}Si beam from Pelletron plus LINAC
Mr. Ratan Kumar Singh, M. S. University, Baroda	Study of heavy ion induced fusion/fission reactions around the Coulomb barrier using ^{16}O and ^{12}C
Ms. Kavita Rani, Panjab University, Chandigarh	Measurement of quasi-elastic process at near barrier energies using ^{28}Si beam
Mr. Sunil Prajapati, Bareilly College, Bareilly	Study of heavy ion induced reactions at Pelletron energies using ^{13}C beam
Prof. Pralay Maiti, School of Materials Science and Technology, IIT (BHU), Varanasi	Study of porous polymeric materials using ^{197}Au ion beam
DOS, ISRO, Bangalore	Tests on micro-electronic devices
DOS, SCL, Panjab	Tests on micro-electronic devices
DOS, SAC, ISRO, Ahmedabad	Tests on micro-electronic devices

4.1.2 Maintenance and servicing activities of GPSC facility

(with technical support from the Vacuum Laboratory and the Mechanical Workshop)

Some of the technical issues related to the high vacuum pumping and the mechanical parts of the rotating arms in GPSC were addressed and resolved by the concerned facility support groups. Due to misalignment, the height of the detector arms had become offset by about 2 mm out of plane over the last few years. The three alignment screws of the individual arms were adjusted to regain coplanarity of the arms. Both the arms are now aligned to an accuracy of 200 µm. The target ladder, used previously, had tilted off the vertical line and the Teflon bush, used to fix it to the central shaft of the chamber, was not able to keep it in the aligned position.

There was a misalignment in the horizontal direction among the different target positions with respect to the beam position. The Teflon bush isolates the target ladder from the chamber body so that the target current can be measured to minimize the chance of beam particles hitting the target ladder. A new Teflon bush and two new target ladders were fabricated in-house. The new target ladders are lightweight and possess all features of the previous ladder. These target ladders were aligned with respect to the beam axis and fixed to the central shaft through the Teflon bush within acceptable accuracy.

The GPSC vacuum system is more than 30 years old. Many vacuum-related problems have been cropping up from time to time for the last few years. The leakage through a Viton gasket, connected to the backing line of the Diffusion Pump (DP) was resolved by making a special gasket in-house. The high vacuum valve which isolates the chamber from the DP had a major leakage. This problem was addressed temporarily by adjusting the alignment of the piston used in the valve. The facility support group from the Vacuum Laboratory and the Machine Shop provided all these services.

4.1.3 Maintenance and servicing activities of NAND facility

(with technical support from the Electronics Laboratory and the Beam Transport Group)

Dust accumulation leads to substantial deterioration in the performance of the electronics modules quite often. A systematic cleaning and servicing of the signal processing electronics of the NAND facility was carried out. All the NIM-based electronics modules used in the NAND data room, especially the home-made integrated Pulse Shape Discriminator (PSD) modules for the neutron detectors were dismantled and cleaned. The set values of the low-level threshold, zero cross over etc. of the PSDs were noted beforehand to maintain the reference. These modules, along with the NIM bins and the cooling fans were cleaned with compressed air and tested thoroughly for their performance. The problems of dry-soldering were attended to wherever required. All the modules were re-installed and connected back with the respective detector signals. Satisfactory performance of the entire system was ensured by testing the same with standard radioactive sources.

Dust accumulation and presence of humidity lead to more serious problems in high voltage power supplies and pre-amplifier power supplies of the neutron detector, which are placed in the beam hall. Routine cleaning and servicing of both the indigenously developed and commercial multi-channel high voltage power supplies were carried out after dismantling those from the respective racks. After cleaning with compressed air, performance of all the individual channels of the power supplies were verified with high voltage probes. The high voltage connections to the respective neutron detector PMTs were restored and performance of the detectors was checked.

4.1.4 Testing of NAND array for the measurement of neutrons above 10 MeV

The NAND facility had been designed mainly for the studies of the dynamics of heavy ion induced fusion-fission reactions near the Coulomb barrier. NAND can also be used for various other aspects of heavy ion-induced reactions in the low and medium energy regime. One of the major nuclear processes that comes up as we go above the Coulomb barrier is the pre-equilibrium emission of particles from the di-nuclear system formed just after the nucleus-nucleus collision. Such energy domains are accessible for lighter projectiles like O, F, etc. with the beam energy available with the booster LINAC. The energy of the pre-equilibrium neutrons are generally higher - as high as 25 – 30 MeV. On the other hand, the energy of neutrons emitted in a typical fusion-fission reaction lies between few 100s of keV to about 10 MeV, with the average energy around 2 MeV. The input dynamic range of the custom-made signal processing electronics (PSD) of NAND is limited up to 10 – 12 MeV neutrons. In order to optimize the available electronics for the measurement of pre-equilibrium neutrons, a systematic study was carried out by reducing the PMT gain through reduction of applied bias voltage. The pulse height of the anode signal was varied by varying the applied PMT bias and the performance of the electronics module was studied under each bias condition. This study was carried out using a ^{252}Cf neutron source by using the Time of Flight (TOF) method. A BaF_2 detector, placed close to the source at the target position of the NAND scattering chamber, was used as the start detector and a neutron detector of the NAND set up was used as the stop detector. The timing as well as the pulse shape discrimination characteristics of the system were thoroughly evaluated. Table 4.1.4 shows how the Figure of Merit (FOM) of pulse shape discrimination and the time resolution of the system (which includes the time resolution of the detectors as well as the electronics) varies at different PMT signal strength, generated by varying the PMT bias. As it is shown in the table, there is no considerable deterioration in the timing and pulse shape discrimination properties of the system as the PMT signal height is reduced by a factor of 5 to accommodate neutrons of energy up to ~32 MeV. These results encourage the usage of NAND for the studies of pre-equilibrium neutrons in future.

Table 4.1.4: Results of the measurements with varying gain of the PMT.

PMT signal (mV)	Dynamic range	FOM (n-γ)	Time resolution, ΔT (ns)
500	~10 MeV	1.6	2.7
200	~18 MeV	1.7	2.5
150	~23 MeV	1.7	2.3
100	~32 MeV	1.7	2.0

4.1.5 Performance results of NAND array

An article on the performance results of the NAND was published in Nucl. Instrum. Methods A [1]. This paper contains technical discussion of all the major sub-components of the array, the design features, individual detector performance and tuning of electronics and its performance using offline and online experiments. To demonstrate performance of the array for high-precision measurements in heavy and super heavy mass regions, a comparison of results between NAND and another smaller detector array facility was made. Results of mass gated neutron multiplicity, measured in super heavy mass region, from the two facilities were compared here [2,3]. In Ref. [3], neutron multiplicities associated with symmetric and asymmetric mass division of the compound nucleus ^{258}Rf were measured using the reaction ^{50}Ti+^{208}Pb at E_{lab} = 294 MeV. A similar reaction ^{48}Ti+^{208}Pb at E_{lab} = 275 MeV was studied using the NAND array [2]. The fragment mass-gated pre-scission neutron multiplicity (M_{pre}), post-scission neutron multiplicity (M_{post}) and the fission transient time delay (τ), extracted from these measurements are summarized in Table 4.1.5. The marginal increase in neutron multiplicities in the reaction ^{50}Ti+^{208}Pb can be attributed to the excess excitation energy of the compound nucleus. The errors quoted for these two measurements differ remarkably. For instance, in Ref. [3] the pre-scission neutron multiplicities associated with symmetric and asymmetric mass components were reported with very large uncertainties (>35%). In contrast, the NAND measurement produced results with less than 5% uncertainty. The NAND experiment was performed with an average beam current of 0.3 pnA but the number of detectors was more. The consistency in the experimental observables and similar interpretation of underlying physical processes in these two independent measurements demonstrate the relevance of the NAND for high precision measurements in heavy and super heavy mass regions.

Table 4.1.5: Comparative results on neutron multiplicity measurements in heavy mass region carried out using NAND [2] and RIPEN [3] facilities.

System	Energy (MeV)	Asymmetric mass cut		Symmetric mass cut		Delay (τ) (zs)
		M_{pre}	M_{post}	M_{pre}	M_{post}	
^{50}Ti+^{208}Pb [3]	294	_	6.3 ± 0.6	2.2 ± 0.8	6.8 ± 0.4	~45
^{48}Ti+^{208}Pb [2]	275	1.66 ± 0.07	5.32 ± 0.05	2.23 ± 0.07	6.02 ± 0.07	~67

REFERENCES

[1] N. Saneesh *et al.,* Nucl. Instrum. Methods A **986**, 164754 (2021).

[2] M. Thakur *et al.,* Phy. Rev. C **98**, 014606 (2018).

[3] S. Appannababu *et al.,* Phy. Rev. C **94**, 044618 (2016).

4.2 GAMMA DETECTOR ARRAYS: GDA and INGA

Yashraj, R. K. Gurjar, Indu Bala, Kusum Rani, R. Kumar, S. Muralithar and R. P. Singh

4.2.1 Indian National Gamma Array (INGA)

In order to migrate the Data Acquisition System (DAS) to VME, the purchase orders for ADC, TDC and Crates were placed. A new VME-based DAS, consisting of global event trigger and crate controller and the software developed in-house, is being tested in the INGA using ^{152}Eu γ-source in singles and coincidence mode.

Five experiments were carried out for nuclear structure studies. An in-beam experiment, using the existing CsI array, electronics (preamplifier developed by A. Jhingan) and the scattering chamber is being planned to study particle-γ coincidence method. Simulation of the Charged Particle Detector Array (CPDA) and testing of CsI with a radiation source were carried out for submitting an SERB project.

4.2.2 LN2 filling system

R. N. Dutt, Ruby Santhi, Yashraj, S. Muralithar and R. P. Singh

New LN2 sensors (PT100) were installed at the outlet of the Clover detectors. A new LN2 control system using industrial modules, based on MODBUS standard and RS485 serial backplane for communication, was procured as per custom-design. This is being used for cooling the Clover germanium detectors replacing the old controller. The control system incorporates Graphic User Interface (GUI) based on LabView software for control and automation. The GUI and "Autofill" routines are being updated.

4.2.3 In-beam test of the plunger facility in INGA

Testing of the new plunger facility was completed successfully in an in-beam experiment in August 2020. Fig. 4.2.3.1 shows assembling of the new plunger device.

Fig. 4.2.3.1: Plunger target-stopper assembly (left) and assembled plunger device inside the scattering chamber made of glass and with a diameter of 4 cm (right).

The reaction ^{14}N+^{93}Nb at E_{lab} = 56 MeV was studied in the test. In this reaction, high spin states of ^{104}Cd and ^{104}Ag were mainly populated. Lifetime measurements in ^{104}Cd, using the plunger device, had been done twice earlier - using the conventional decay curve and the differential decay curve techniques by Muller *et al.* [1] and using the differential technique by N. Boelaert *et al.* [2]. A coincidence spectrum from our measurements is shown in Fig. 4.2.3.2 with a gate on the shifted component of 834 keV transition ($4^+ \rightarrow 2^+$) in ^{104}Cd. Shifted and unshifted peaks of different transitions at various distances can be seen. In particular, the components of 658 keV transition ($2^+ \rightarrow 0^+$) just below the 834 KeV transition is very clear. Preliminary analysis yields a mean life of about 8.2 (8) ps for the 2^+ state in ^{104}Cd. transition

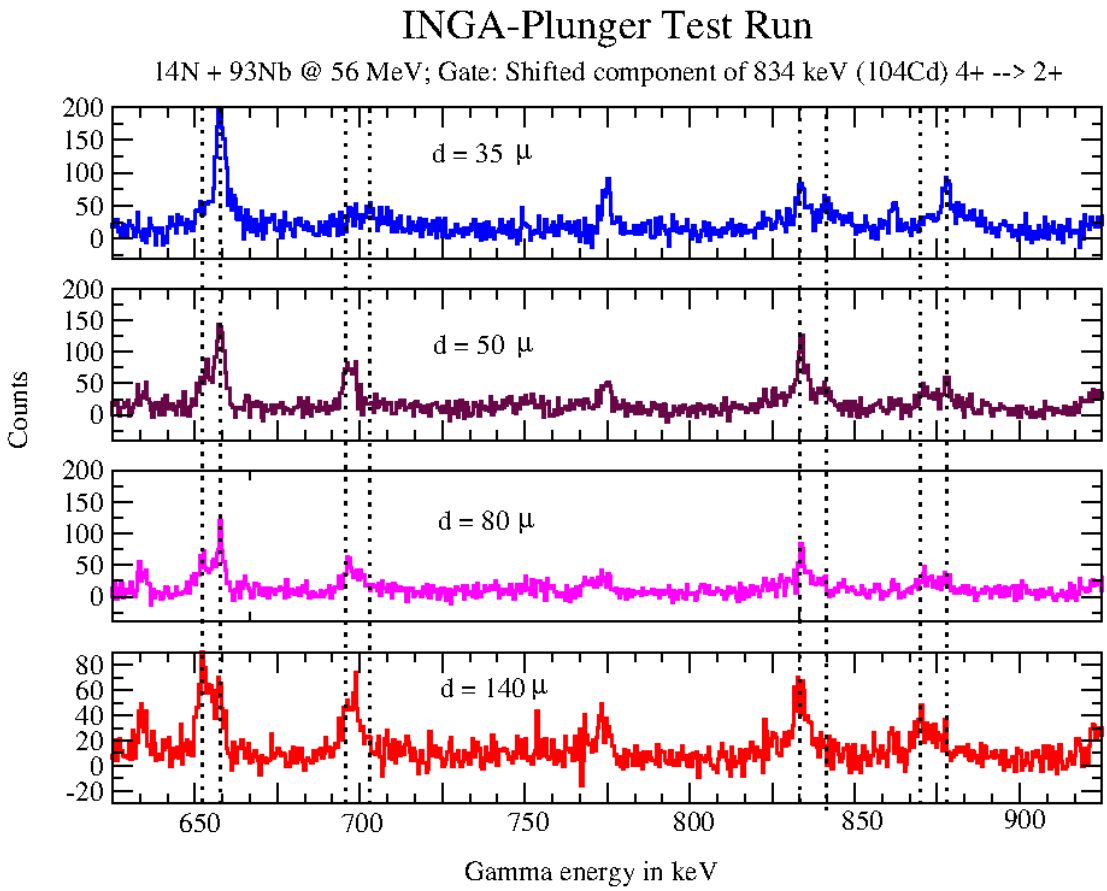

Fig. 4.2.3.2: A sample spectrum from the plunger test.

REFERENCES

[1] G. Muller *et al.*, Phys. Rev. C **64**, 014305 (2001).

[2] N. Boelaert *et al.*, Phys. Rev. C **75**, 054311 (2007).

4.3 RECOIL MASS SPECTROMETERS

4.3.1 Heavy Ion Reaction Analyzer (HIRA)

S. Nath, J. Gehlot, Gonika, T. Varughese and N. Madhavan

HIRA facility was used in six experimental runs, all of which were part of student thesis proposals. This was despite the COVID-19 related initial lockdown and the gradual opening up that followed. Two-thirds of the Nuclear Physics experimental runs were carried out using the HIRA in the past year.

The first experimental run involved the measurements of fusion and quasi-elastic back-scattering / transfer cross sections around and below the Coulomb barrier in $^{16}O+^{142}Ce$ system (Rohan Biswas, research scholar from IUAC / JNU). Rohan Biswas *et al.* also developed a simulation code based on Monte Carlo techniques to calculate the transmission efficiency for target-like particles through the HIRA.

Above barrier and sub-barrier cross section measurements were carried out for $^{19}F+^{142,150}Nd$ systems (A. C. Visakh, research scholar from Central University of Kerala, Kasaragod) in the second and final run of thesis work. The analysis and interpretations of the earlier measurements involving near and sub-barrier (down to more than 10 % below the barrier) cross sections for the systems $^{16}O+^{142,150}Nd$ have been carried out and the draft manuscript is being prepared.

In order to study the effect of neutron number in the formation and survival of evaporation residues (Ers), near and sub-barrier cross section measurements were carried out for the $^{12}C+^{180,184,186}W$ systems (Sanila S., research scholar from Calicut University). For comparison / calibration, a few energy points were taken for the $^{12}C+^{182}W$ system. As the ER energies below the barrier were very low, extremely thin targets were used. The available target thickness decided how low the measurements could be carried out for each system.

Quasi-elastic back-scattering and ER cross section measurements were carried out for $^{19}F+^{64,68}Zn$ systems (Shoaib Noor, research scholar from Thapar University) around and below the barrier. The effect of positive Q-

value transfer channels on sub-barrier cross section enhancement was probed in this experiment. Time-of-Flight, energy loss and position signals were collectively used to filter the various groups of scattered beam-like particles and to select the ERs.

Near and sub-barrier fusion and quasi-elastic back-scattering cross section measurements were carried out for the $^{28}Si+^{116,120,124}Sn$ systems (Anjali Rani, research scholar from Delhi University) in two runs (above barrier data taken after Pelletron maintenance and the associated stripper foil change) to study the effect of neutron number in the target (with closed proton shell, Z = 50). Correspondingly, the neutron number of the compound nucleus (CN) spans from below the closed shell (N = 82) to well above it.

The focal plane detector window foil (0.5 μm thick, 150×50 mm^2 cross section), which broke during one of the experiments, was replaced the same day. The focal plane detector system in the HIRA was tested and calibrated with α-particles from a radioactive source.

Two research scholars were awarded Ph. D. degree based on the work carried out using the HIRA in earlier years.

4.3.2 HYbrid Recoil mass Analyzer (HYRA)

N. Madhavan, S. Nath, J. Gehlot, T. Varughese, Gonika

As beams from the Pelletron + SC-LINAC combined facility were not available for experiments the past year, pending experiments could not be scheduled using the HYRA facility. However, the group was involved in taking several experiments in HIRA as explained in the previous section. The compact MWPC detector, developed for the proposed isomer decay setup in the HYRA, was tested and calibrated using an α-particle source. All the signals (namely, four position signals, energy loss (ΔE) and timing signal from the anode) were found to be in order. A facility test with beam will be taken up prior to using it in the isomer decay experiments. The presently used large area MWPC was also tested using an α-particle source.

The analysis and interpretations of the ER excitation function data collected in January 2020 during the LINAC campaign (Devinder Pal Kaur, research scholar from Panjab University) for the $^{48}Ti+^{140,142}Ce$ systems have been completed and the manuscript is being drafted.

A project proposal has been submitted to SERB (Principal Investigator: Jagdish Gehlot) for the development of a comprehensive detector system (and associated electronics) for the HYRA focal plane for ER-tagged decay studies in the gas-filled mode.

Three research scholars were awarded Ph.D. based on the work carried out using the HYRA in earlier years.

Dr. Kyaw Thiha, Lecturer, Department of Physics, Mandalay University, Myanmar, who had applied for India Science and Research Fellowship (ISRF-2020, offered by the Department of Science and Technology) in consultation with Dr. N. Madhavan as the mentor and IUAC as the Host Institute, has been selected as one of the 40 successful candidates from Afghanistan, Bangladesh, Bhutan, Maldives, Myanmar, Nepal and Sri Lanka.

4.4 MATERIALS SCIENCE FACILITIES

A. Tripathi, D. Kabiraj, K. Asokan, V.V. Sivakumar, Fouran Singh, S.A. Khan, P. K. Kulriya, I. Sulania, R.C. Meena, and A. Mishra

The materials science facilities are supporting research programmes of a large number of users from different universities and research institutions. Last year, after the Covid lockdown, the facilities became operation again in September and user experiments were being scheduled since then. A total of 18 user experiments spread over 64 shifts and were performed this year and there were no major breakdown of facilities resulting in beam time loss in materials science beamline in beamhall I. BTA experiments associated with students' Ph.D. programmes continued to get priority with 10 runs spread over 34 shifts were completed. Though the swift heavy ion (SHI) irradiation and related experiments mostly utilize irradiation chamber in the materials science beamlines in beamhall-I, one experiment involving low fluence irradiation was performed in the GPSC. The details of the experiments being done in areas of SHI induced materials modification and characterization are given in Section 5.2 and related publication are given in sec 6.7. Besides irradiation facilities, materials science group is also providing many materials synthesis and characterization facilities and this year limited off line characterizations were undertaken keeping Covid protocols in place.

Special emphasis is given on organising workshops and schools on specialized topics so that the users are familiar with state of art experiments and facilities. Due to COVID situation the activities were undertaken in an online mode. 6th International Conference on Ion Beams in Materials Engineering and Characterization (Dec 8-11, 2020) and International School on Ion Beams in Materials Science (Dec 1-5, 2020) were organized this year and details are given in section 6.

4.4.1 Maintenance of Irradiation chamber in Beam Hall I

I Sulania, S A Khan and A. Tripathi

The HV experimental chamber in Materials Science beamline in BH1 was used by a large number of materials science users for their experiments. In total, 18 experiments have been carried out utilizing 61 shifts by 18 users in BH1 experimental chamber. There were a few maintenance works carried out during 2020-21. The scroll pump was replaced with a new vacuum pump as users were facing issues with obtaining low vacuum. Some problem was reported with BLV 51 and 52 beam line valves controlled remotely from control room. This is being taken care by Dr. Kundan Singh.

4.4.2. Material Synthesis and Microscopy laboratory.

Indra Sulania, Saif Ahmed Khan and V. V. Siva Kumar

The laboratory has few synthesis facilities for the growth of thin films and nanopowders and some characterization facilities such as Scanning Electron Microscope, Scanning Probe Microscope, Optical Microscope, UV-Vis Spectrophotometer and Contact Angle measurement set-up. The facilities are in proper working condition. The Microscopy facilities have been extensively utilized by IUAC user community belonging to different universities/institutes. However this year, the user activity was limited and a total of 268 samples of 54 users were characterized using the different systems.

The scanning electron microscope was utilized for characterizing samples of about 10 users with most of them being from IUAC. This was due to limited visits by outside users since the year was affected due to pandemic related restrictions. In this period, 39 samples were characterized for composition estimates using attached energy dispersive x-ray spectroscopy system. Conducting thin film deposition on the surface using coater was not required since the characterized samples did not show charging problems during microscopy.

Most of the Scanning Probe Microscope modes such as AFM, MFM, C-AFM, STM, STS and F-d mode etc are available at IUAC and used in user experiments. This year, due to corona pandemic, a total number of 55 samples were scanned with SPM for 12 users in AFM and STM modes. The facility is working satisfactorily and no major maintenance was required.

The laboratory has a high-end Optical Microscope from Zeiss, which can magnify the images up to 100x. It is mostly used as a tool to predetermine the sample's area before performing the SPM measurements. It is especially useful to track the single or multilayer graphene flakes etc. The Optical Microscope system was utilized for characterizing 35 samples of 5 users.

The UV-Vis Spectrophotometer which was procured from Hitachi, is capable of doing measurements in Absorbance/Transmission mode. A mouse connector in CPU of UV-Vis spectrophotometer set-up had some issues. It was rectified this year, by connecting a USB dongle/mouse connector. Further, CPU connection was established to the UV-Vis setup and contact angle measurement set up to avoid shutting down of PC due to power failure. The UV-Vis spectrophotometer was used to characterize 105 samples of 14 users.

4.4.2.1 Contact Angle Measurement Set-up.

Indra Sulania

The laboratory has a unique Instrument, Drop Shape Analyzer, DSA 100, from Kruss GmbH – Germany. It is a high-quality system for knowing the wetting and adhesion solid surfaces with water drop. From the basic unit for precise measurement of the contact angle to the fully automatic expert instrument for serial measurement of surface free energy. When an interface exists between a liquid and a solid, the angle between the surface of the liquid and the outline of the contact surface is described as the contact angle θ (lower case theta). The contact angle (wetting angle) is a measure of the wettability of a solid by a liquid. This year, it was utilized by 3 users scanning 34 samples. The set-up is working satisfactorily and no major maintenance was required.

4.4.3 Status of the Facilities Available in the Transport Lab

Ramcharan Meena, Anuradha, Ashish Kumar, Razia Nonjgai, K. Asokan

To characterize the transport properties of thin film or bulk compounds, various characterization facilities are available at IUAC. To know the type of charge carriers and concentration of semiconductors, the Hall effect measurements set is available. It works on room temperature as well as liquid nitrogen temperature. The resistivity behaviors of the samples are also measured within the temperature range from 10K-400K using the cryo-cooler and liquid nitrogen cryostat. For low resistive materials, the electrical resistance is measured using the current source and nano-voltmeter and for highly resistive materials electrometer is used. To know the dielectric properties of a material within the frequency range 20Hz-2MHz in the temperature interval 10K-400K, LCR meter is used. We are also having a high-temperature dielectric measurement setup, its works in the temperature range from room temperature to 800^{o}C.

Semiconductor devices characterization is very important equipment for industrial application. We are having a B1500 semiconductor device analyzer to characterize the device at room temperature using the W metal probes. Thermoelectric materials are also characterized using the homemade thermoelectric measurement setup within the temperature range of 90K-450K. Magnetoresistance of the samples are also measured from 80K-450K of the magnetic field range 0-1.7 Tesla.

To synthesize the samples there three types of furnaces available for users: air, vacuum and rapid thermal annealing set up. These furnaces work up to the temperature range of 1200°C. Annealing can be done on both type of samples (bulk and thin films).

There was no major breakdown in any of these facilities except in the cryo-cooler. It was not functioning for four months because of the leak in the high-pressure line of He gas. Now the problem is rectified and the facility is available to the users.

An in-situ electrical transport measurements facility is also available in the lab. Sample /device in-situ characterization is done by I-V, C-V or resistivity measurements. These characterizations are done at various ion fluences and different temperatures using the homemade in-situ ladder.

All the above-mentioned facilities were used by 25 users last year.

4.4.4 TEM Facility Activities

Ambuj Mishra, Abhilash S R and D Kabiraj

Energetic ion beams play a crucial role in materials modification and so changing their physical properties. TEM is a state-of-the-art technique which can investigate morphological, structural and compositional modifications in a material. The role of IUAC TEM and TEM sample preparation facility has been described herewith which have been used by various users to understand ion beam effect in materials modification. Time utilization (in days) of TEM Facility for 2020-21 is shown in the Fig.1.

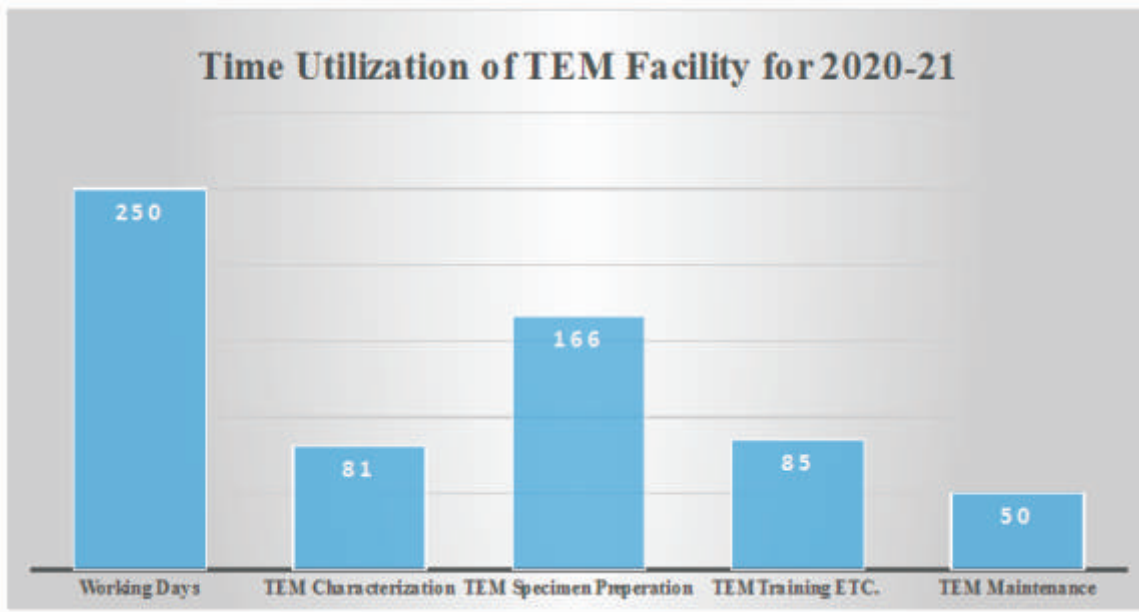

Fig.1: Time Utilization (in days) of TEM Facility for 2020-21.

TEM Specimen Preparation

TEM specimen preparation facility is equipped with Ultrasonic bath, Hot Plate, Traditional Lapping/Grinding Tools, Dimple Grinder, Diamond Wire Saw and Precision Ion Polishing System (PIPS). All these instruments are regularly used for TEM sample preparation. TEM, Cross-sectional TEM (XTEM) and Powder samples on TEM Grids can be prepared here for TEM characterization. Utilization of this facility is shown in the Fig.1.

TEM

Maintenance of TEM very important for smooth operation and is done as and when required. Some of the regular TEM maintenance activities undertaken are Chiller water replacement, Bake-out process, HT

conditioning after Bake-out process, ACD heating, Camera warmup etc. This year TEM bake-outs have been done in the month of August 2020, October 2020, November 2020 and February 2021. Each time, after these bake-outs, HT conditioning has been done. All TEM facility Log books, TEM maintenance reports/logs and TEM user data backup have been kept updated time to time.

This year several samples have been characterized for TEM, HRTEM, Selected Area Electron Diffraction (SAED). Some of the research works using IUAC TEM facility which are published this year are briefly described below:

(i) Study of morphological and structural properties of amorphization/ crystallization at the interfaces of thin films

G. Maity *et. al*. has reported on the morphology of crystalline Si surfaces in Al/a-Si bilayer thin films under ion beam irradiation at 100°C [G. Maity *et. al.*, Journal of Applied Physics 129 (2021) 045301]. Best crystallization has been achieved at a fluence of 1×10^{12} ions cm^{-2} which is evident from the Micro-Raman and TEM studies. In the Fig.2(b) and 2(c), the XTEM images of the pristine sample [i.e., c-Al(50 nm)/a-Si(150 nm)] and the bilayer thin film irradiated at a fluence of 5×10^{12} ions cm^{-2} have been shown respectively. A clear sharp interface between a-Si/Al has been seen in the Fig.2(b), whereas three distinct layers, top layer (i.e., unreacted c-Al: ~ 38 nm), bottom layer (a-Si), and an intermediate layer (i.e., diffused layer: ~ 25 nm) have been observed in the Fig.2(c), supporting the irradiation induced changes. In the Fig.2(d), a high resolution TEM (HRTEM) image of a selected area from the intermediate layer has been shown which was recorded to understand the nature of the intermediate layer. A detailed analysis of HRTEM image has shown that this layer predominantly contains c-Si along with a mixture of c-Al and c-Si at some places. The local high temperature due to ion irradiation and an elevated substrate temperature facilitate the accumulation of Si near Al grain boundaries and upon sufficient accumulation of Si atoms, the crystallization of Si gets initiated.

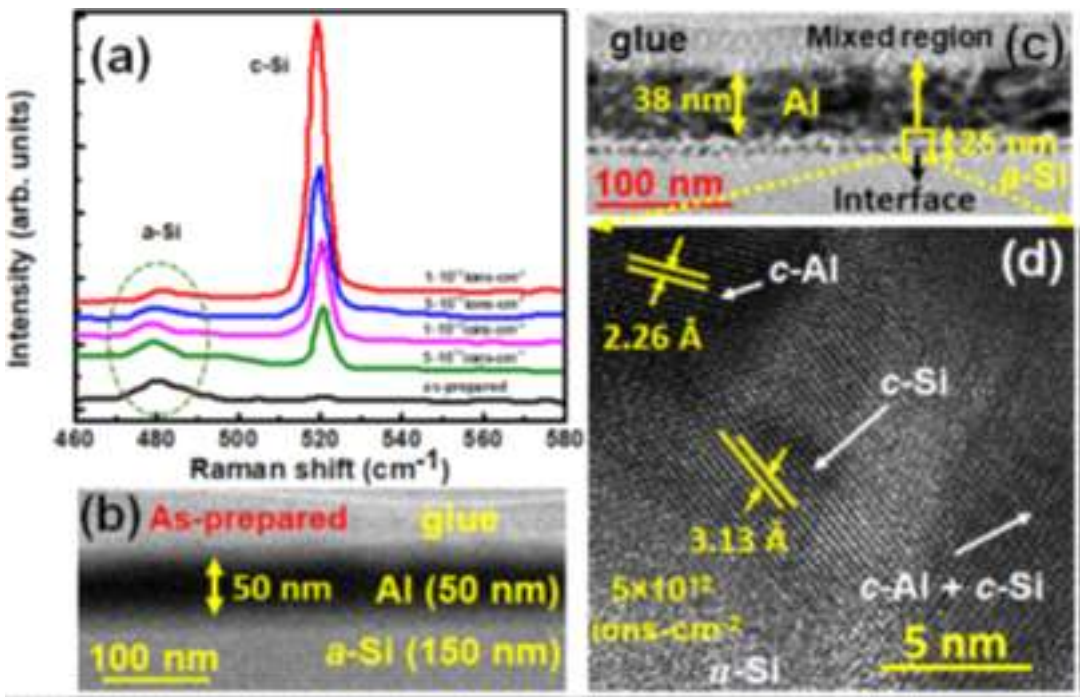

Fig 2: *(a) Micro-Raman spectra of the pristine and irradiated c-Al/a-Si samples. (b) XTEM image of the pristine sample. (c) XTEM image of the sample irradiated at the ion fluence of 5×10^{12} ions cm^{-2}. (d) HRTEM image of a selected area from the middle layer of the irradiated (at a fluence of 5×10^{12} ions cm^{-2}) sample.*

(ii) Study of morphological and structural properties of quantum dots (QDs), nanowires (NWs) and 2D materials

Abid et. al. has fabricated and investigated a novel photodetector based on a WS_2 quantum dots and reduced graphene oxide (RGO) (WS_2-QDs/RGO) heterostructure [Abid *et. al.*, ACS Appl. Mater. Interfaces 2020, 12, 39730−39744]. The morphology of materials and WS_2-QDs/RGO heterostructure have been examined using IUAC JEOL JEM F-200 transmission electron microscope. TEM analyses of GO flake (a), bulk WS_2 (b), and WS_2-QDs at different magnifications (c−e) is shown in the Fig.3. In the TEM image (Fig.3(a)), few wrinkles

are visible in the GO flakes. In the Fig.3(b), the multilayered WS_2 flake can be observed with the flake size of ~ 2 µm. After the solvothermal process, these WS_2 flakes breaks into WS_2-QDs with the size ranging between 5 to 7 nm as shown in the Fig.3(c). The HRTEM images in Fig.3(d)-(e), show the crystalline nature of the QDs.

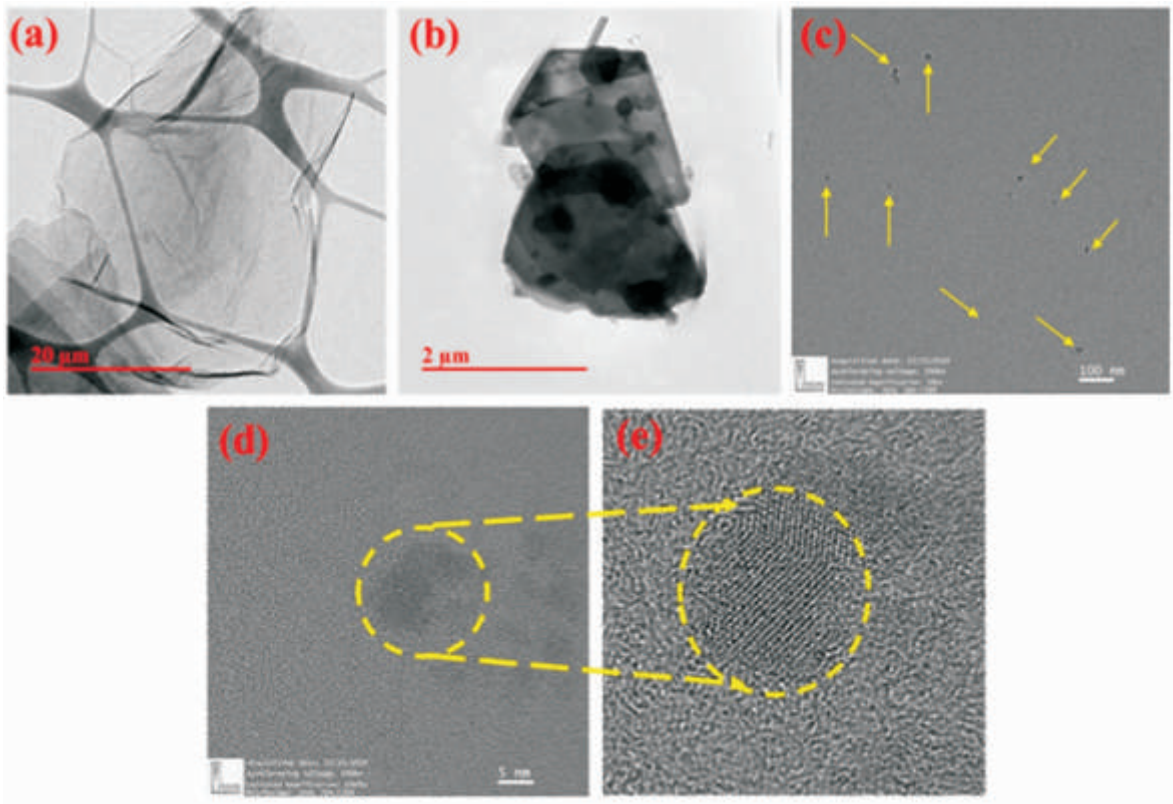

Fig 3: *TEM images of (a) GO flake, (b) bulk WS_2, and (c−e) WS_2-QDs at different magnifications.*

Honey Mittal *et. al*. have synthesized a novel $MoSe_2$-PPy nanocomposite using in situ oxidative polymerization method [Honey Mittal *et. al.*, Separation and Purification Technology 254 (2021) 117508.]. In the Fig.4(a), the HRTEM image of MSEPY nanocomposite has been shown which confirmed the interaction between $MoSe_2$ and PPy. The PPy and $MoSe_2$ are found in the form of nanoparticles and nanosheets, respectively. It has been clearly observed that the $MoSe_2$ nanosheets have a very thin layer with a smooth surface. The hexagonal lattice fringes have been observed in the HRTEM image with a lattice spacing of 0.28 nm which is corresponding to the (100) plane of $MoSe_2$. The average diameter of PPy nanoparticle has been found to be 105.83 nm. In the Fig.4(b), The SAED pattern shows two diffraction rings corresponding to the inter-planar distances of 0.263 nm and 0.145 nm which exhibit the crystal planes of (100) and (110) of $MoSe_2$, respectively.

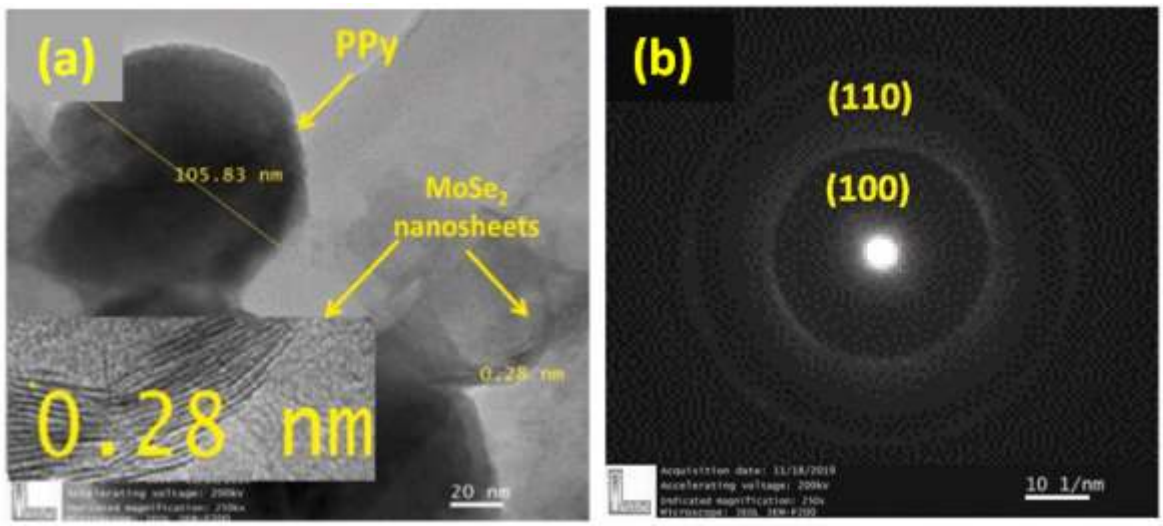

Fig 4: *(a) TEM of MSEPY (inset showed the enlarged portion of $MoSe_2$ nanosheets) and (b) SAED pattern of MSEPY [3].*

To improve the optical and electrical properties of graphene quantum dots (GQDs), Shikha Wadhwa *et. al*. has synthesized graphene quantum dots–gold (GQD-Au) hybrid nanoparticles of the size of ranging between ~5-100 nm [Shikha Wadhwa *et. al*. MethodsX 7 (2020) 100963]. The synthesis of GQD-Au hybrid nanoparticles has been confirmed by the HRTEM micrograph shown in the Fig.5 which indicates the dispersed spherical particle formation with the particle size ranging between ~5-100 nm. In the inset of the Fig.5, gold lattice plane (111) corresponding to the inter-planar distance of 0.233 nm in the inner region and lattice plane (100) of graphitic carbon corresponding to the inter-planar distance of 0.243 nm on the surface of hybrid nanoparticles have been observed which indicated the formation of a core/shell AuNPs@GQD structure.

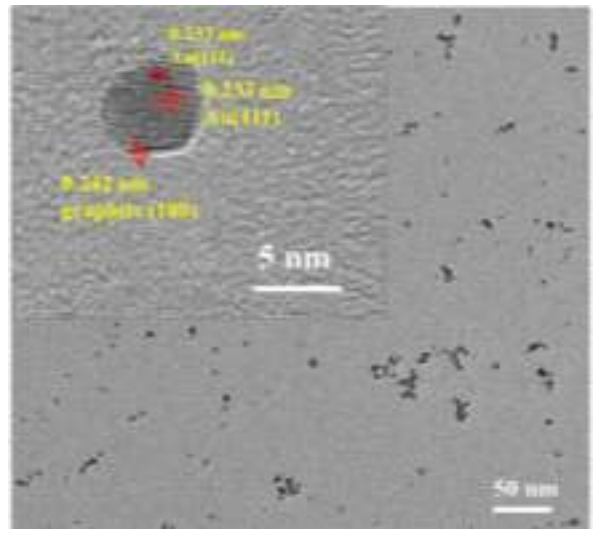

Fig 5: *HRTEM micrograph of GQD-Au hybrid nanoparticles [4].*

(iii) Study of morphological and structural properties of thin films and powder samples

The TEM, HRTEM and SAED measurements have been performed to find out the particle size distribution and crystallinity of Sn doped In_2O_3 (In_{2-x} Sn_xO_3; $0.0 \leqslant x \leqslant 0.25$) synthesized by solid state reaction method [Afroz Khan *et. al*. Solid State Sciences 109 (2020) 106436]. In Fig.6(a) and 6(e), the TEM images for x = 0.1 and x = 0.2 have confirmed the spherical nature with some agglomeration of nanograined powder. The particle size decreases with increasing concentration of Sn as shown in these TEM images. From the Fig.6(d) and 6(h), the particle sizes have been found to be 81.72 nm and 79.17 nm for the samples x = 0.1 and 0.2, respectively. The SAED images presented in the Fig.6(c) and 6(g) confirms cubic bixbyite structure and the successful incorporation of Sn into the In_2O_3 crystal lattice. The obtained distinct rings in the SAED images have revealed the formation of nanocrystalline grains in the powder samples. In the Fig.6(b) and 6(f), the d-spacing in two directions have been measured to be 2.91 Å which indicates the (222) plane for x = 0.1 and 2.91 Å & 1.78 Å which correspond the (222) & (440) planes for x = 0.2 of In_2O_3, respectively.

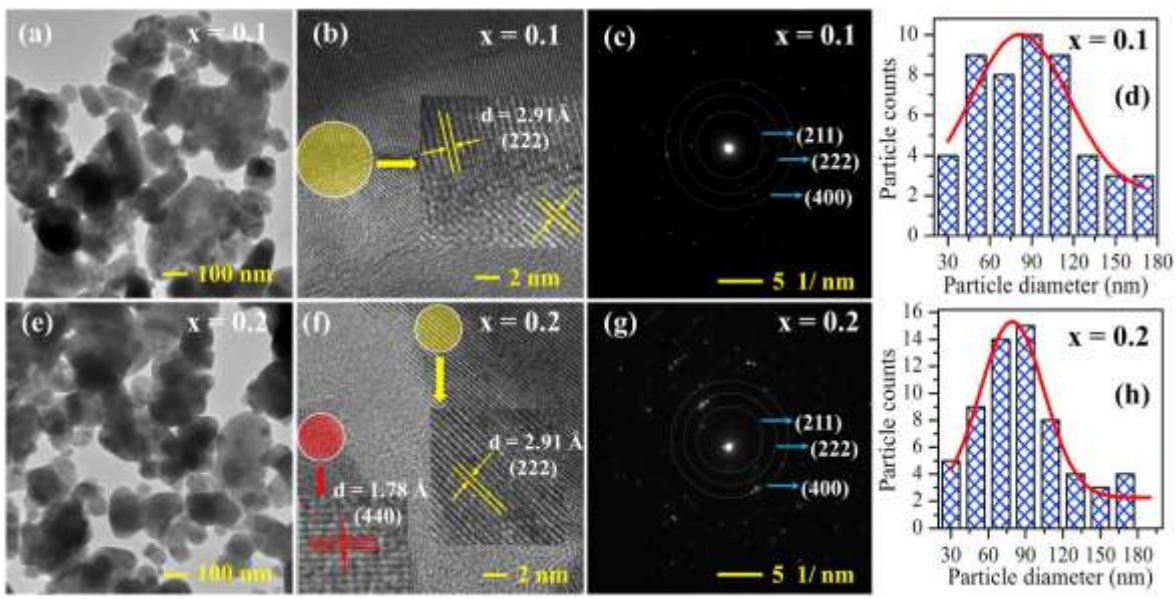

Fig 6: *(a, e) TEM images, (b, f) HRTEM fringe patterns; insets show the zoomed region with inter-planer spacing related to particular plane, (c, g) SAED patterns and (d, h) particle size distributions of $In_{2-x}Sn_xO_3$ nanocrystalline samples for x = 0.1 and 0.2 respectively [5].*

Saurabh K. Sharma *et. al*. have investigated the grain size driven effects on electronic excitation-induced structural modifications in nanocrystalline (NC) $Nd_2Zr_2O_7$ on irradiation with 100 MeV iodine ions [Saurabh K. Sharma *et. al*. Journal of Applied Physics 129 (2021) 115902]. To investigate the effect of annealing temperature on the microstructure, TEM studies have been performed on the pristine samples. TEM images, HRTEM images, and SAED patterns of pristine P6, P10, and P13 samples of NC-$Nd_2Zr_2O_7$ are shown in Fig.6(a)−6(i). The average nanoparticle sizes are measured to be ~ 40 nm, ~ 80 nm and ~ 175 nm for the P6, P10, and P13 samples, respectively, as depicted in the Fig.6(a)−6(c). In the HRTEM image of P6, the regular lattice fringes with an interplanar distance of ~ 0.266 nm and ~ 0.307 nm have been observed which correspond to the planes (400) and (222), respectively, as indexed in the Fig.6(d). Similarly, the lattice fringes with interplanar distances have been mapped in HRTEM images of P10 and P13 samples as shown in the Fig.6(e) and 6(f). These characteristic lattice fringes belong to both pyrochlore as well as anion-deficient fluorite structures. From the SAED patterns, the pyrochlore superstructure has been confirmed by the presence of a strong diffraction point in a ring pattern of (111) for P6, (311) and (531) for P10, and (311) and (511) for P13 as indexed in the Fig.6(g)−6(i), respectively.

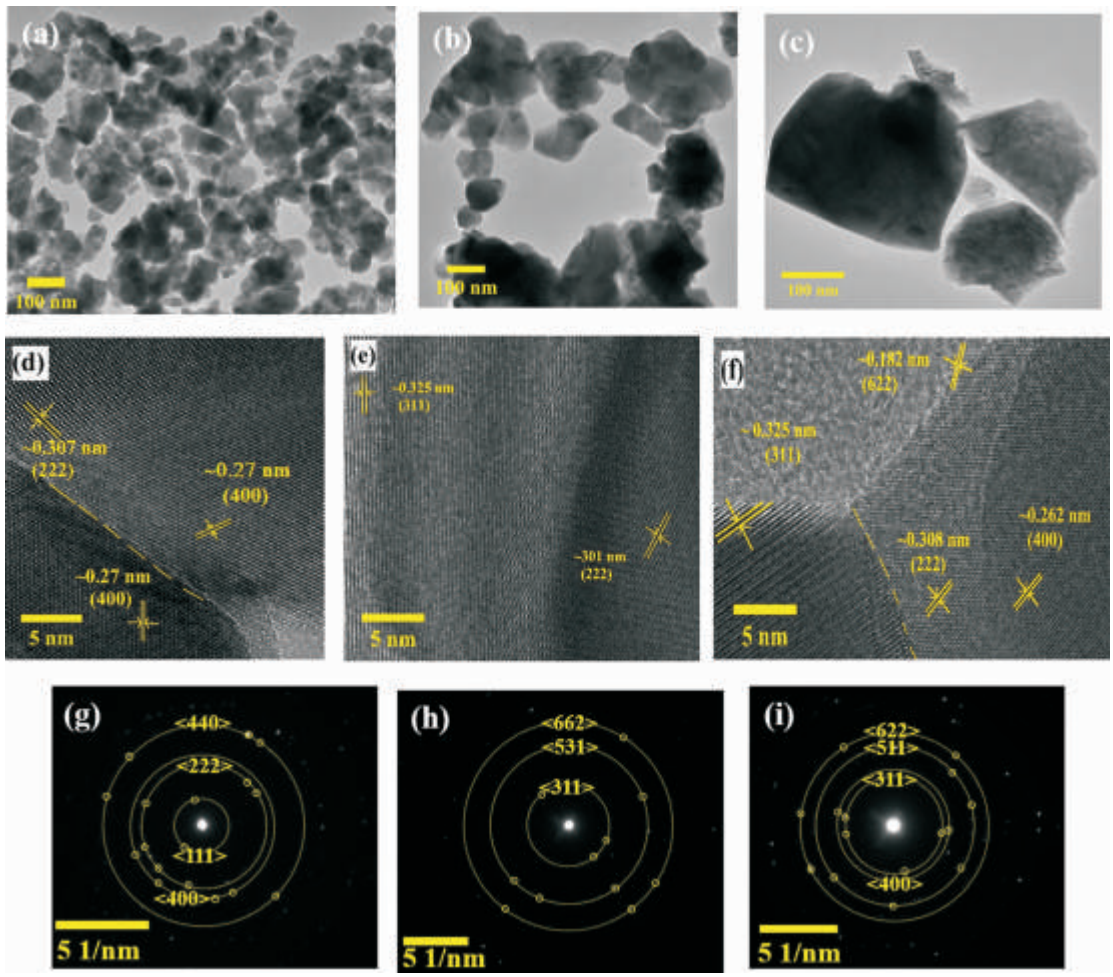

Fig 6: *TEM images of NC-$Nd_2Zr_2O_7$ of samples (a) P6, (b) P10, and (c) P13; HRTEM images of (d) P6, (e) P10, and (f) P13; and SAED patterns of (g) P6, (h) P10, and (i) P13.*

The HRTEM image of irradiated P6 has shown almost amorphous nanoparticles with a small fraction of lattice fringes as observed in the Fig.7(a). These observed lattice fringes with interplanar distances of ~ 0.266 and ~ 0.307 nm exhibit the (400) and (222) planes, respectively. On the contrary, irradiation of P10 and P13 of NC-$Nd_2Zr_2O_7$ results in complete amorphization as demonstrated by HRTEM images in Fig.7(b) and 7(c), respectively.

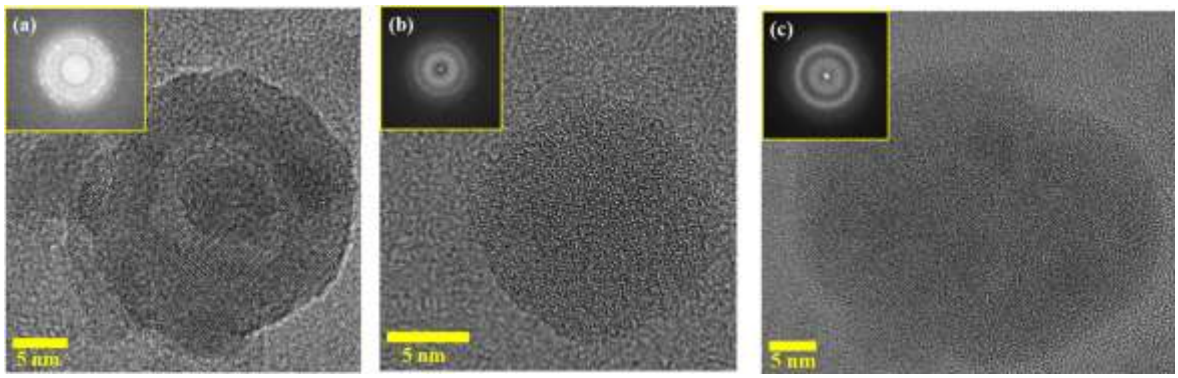

Fig 7: *Plane-view HRTEM images with fast Fourier transformation (FFT) analysis (inset) of copper grids of (a) P6, (b) P10, and (c) P13 irradiated at the fluence of 5×10^{13} ions/cm^2.*

4.5 RADIATION BIOLOGY

4.5.1 Status of the research work done using the Radiation Biology facility

A. Sarma

The Radiation Biology experiments involving accelerated heavy ions are carried out at the dedicated Radiation Biology Beam line of IUAC and utilizing the **ASPIRE** [Automated sample positioning and irradiation system for radiation biology experiments] system. In this system the irradiation of cells by accelerated heavy ions can be done at atmospheric pressure with a set of preset doses. The system is characterized by the dose uniformity over a field of 40 mm diameter within 2% standard deviation. The mean fluence is within 1 % of the electronically measured value at the centre of the field. The characterization of the system has also been done using irradiating SSNTD [CN 85].

The radiation biology laboratory is having the following equipment to facilitate the sample preparation and post irradiation treatments.

(1) Two CO_2 incubators, Two biosafety cabinets, one small laminar flow bench Eppendorf and Plastocraft Refrigerated Centrifuge and a Biotek micro-plate washer.for cell culture and cell sample preparation.

(2) Analytical equipment like Field Inversion Gel electrophoresis, Normal gel electrophoresis, protein gel electrophoresis set up, Image based cell counter Countess [Invitrogen] which also gives information about cell viability and Beckman-Coulter Z2 cell counter, PCR machine, a crude gel documentation system, UV-Vis Spectrophotometer and a Fluorescence microscope, Perkin Elmer Multimode Plate Reader.

Apart from that, LN2 Dewars, -20 deep freezer and other normal refrigerators serve as the storage facilities. The laboratory section has independent Split AC supply isolated from the central AC system. Regular work is going on in the laboratory on Analytical procedures involving gene expression studies using PCR, Western Blot, Fluorescence Immunostaining studies etc by the University Users.

The following are the projects which are undertaken at present

(1) Signaling pathways of activation and secretion of Matrix Metalloproteinases from human lung carcinoma cells after irradiation with carbon ion beam, Payel Dey, Kalyani University

(2) Radio sensitization of human cancer cells using G-quadruplex ligands. Sourav Ghosh, Kalyani University

(3) Carbon nanomaterials as cell radiosensitizers in therapeutics, M. Mukherjee, Amity University.

(4) Evaluation of Radio-protective property of 2,4 di nitrophenol in cellular model against particle radiation. Anant Narayan Bhatt, INMAS.

(5) Chromosomal damage induced by High LET Carbon beam radiation in comparison to gamma radiation in human peripheral blood lymphocytes/ Chinese hamster fibroblast (V79) cells and the effect of Diclofenac sodium in modulating it. Amit Alok, INMAS

(6) DNA damage repair kinetics by a potential countermeasure agent using γ-H2AX/comet assay. Paban K Agrawala, INMAS.

(7) Role of autophagy in High Linear Energy Transfer (LET) radiation induced cell death in normal vs. transformed cells. Mitu Lal, IUAC

(8) Differential cellular response to carbon beam in normal versus transformed cells with special reference to mitochondria. Sweta Sanguri, IUAC

(9) Studies on TLR agonist (mannan) mediated modification in biological radiation response(s) in vitro after carbon beam exposure. Damodar Gupta, INMAS, DRDO

(10) Studies on 2-Deoxy-D-glucose capped Gold-coated magnetic nanoparticles (Au@MFe2O4) for transonic and cancer therapy application. Rajesha Nairy K, K.L.E. Society's P.C. Jabin Science College, Vidya nagar, Hubballi

4.6 ATOMIC AND MOLECULAR PHYSICS

4.6.1 Status of vacuum chamber at 75^0 beam line in LEIBF

D. K. Swami, C.P. Safvan and R P Singh

Atomic physics related x-ray spectroscopy experiments at low energy are performed in vacuum chamber at 75^0 beam line in LEIBF. This year two experiments (10+33 shifts) have been performed in this vacuum chamber. The aim of these experiments are to investigation of heavy-ion atom collision processes in the low energy regime. Two silicon drift x-ray detectors (SDD) for x-ray measurements were used in these experiments. These SDDs detectors were install at 45^0 and 90^0 with respect to ion beam. The experimental resolution of these detectors were 190-200 eV at 5.9 keV. Two Silicon surface barrier detectors were also used for measurements of scattered and back scattered charged particles. In these experiments, Xe (2-5 MeV), H (350 keV), Ne (1.5-4 MeV) and Ar (1.5-4 MeV) ion beams were used. As targets, Ho, Pt, Au, Pb, Bi, Al, Al and Cu on CaF_2 of different thicknesses were used. At a time, 4-5 targets can be used. For the linear and angular motion of the targets, one linear motion feed through and one rotatable axis-360° adjustable stage are mount at the top of the lid respectively. In this experiment, one new collimator (penetrable faraday cup) was installed and aligned at the entrance of the ion beam before the targets. During experiments, vacuum inside the chamber was 10^{-6} - 10^{-7} mbar.

4.6.2 Status of general-purpose atomic physics vacuum chamber (GPAC) at beam hall-II

D. K. Swami and R P Singh

Highly charged ion beam solid collision x-ray spectroscopy experiments at high energy are performed in general purpose atomic physics vacuum chamber (GPAC) at beam hall-II. This year one experiment (10 shifts) have been performed in GPAC. The aim of this experiment is Investigation of heavy-ion atom collision processes in high energy regime. Two silicon drift x-ray detectors (SDD) for x-ray measurements were used in these experiments. These SDDs detectors were install at 45^0 and 90^0 with respect to ion beam. The experimental resolution of these detectors was ~140 eV at 5.9 keV. Two Silicon surface barrier detectors were also used for measurements of scattered and back scattered charged particles. In this experiment, Au and Ni (90-120 MeV) ion beams were used. As a targets, Ni, Cu, Ge and Sn of 40 ug/cm^2 thickness on 20 ug/cm^2 carbon backing of

different thicknesses were used. At a time, 12 targets can be used. During experiments, vacuum inside the chamber was 10^{-6} - 10^{-7} mbar.

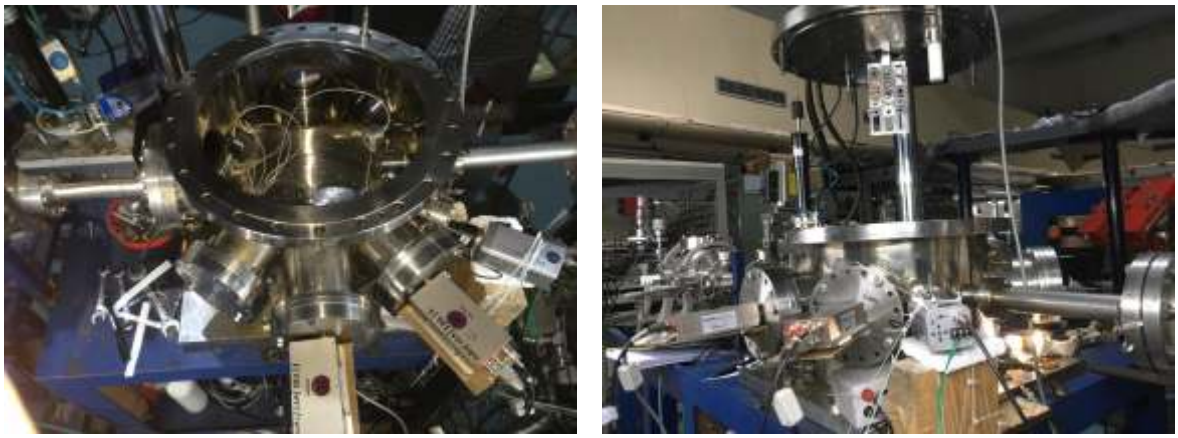

Fig 2: GPAC in beam hall-II.

4.6.3 Status of vacuum chamber at 105^0 beam line in LEIBF

Pragya Bhatt, Aditya Kumar and C P Safvan

An offline facility test was conducted in June 2020 to test the vacuum conditions, detectors signals etc as there was a total shutdown of the molecular physics facility for around two months due to the pandemic. Later, an online facility test was conducted to check whether all the detectors were functioning properly. For this, the ion beams of 50-250 kV/q Ar^{q+} and Xe^{q+} were used on the target atoms/molecules (Ar, N_2, C_2H_2). After all the necessary amendments, the mass and momentum resolution of the spectrometer was obtained to be the same as that before the shutdown of the facility. It was observed that all the systems are working properly except the post collision detector which would be rectified in future.

After the facility test, one of the user experiments was conducted for 50-250 kV/q Xe^{9+} ion interaction with C_2H_2. It was observed in the initial data analysis that the parent molecular ion $C_2H_2^{3+}$ could dissociate via sequential and concerted bond breakup mechanisms as shown in the Dalitz plot in the figure 3.

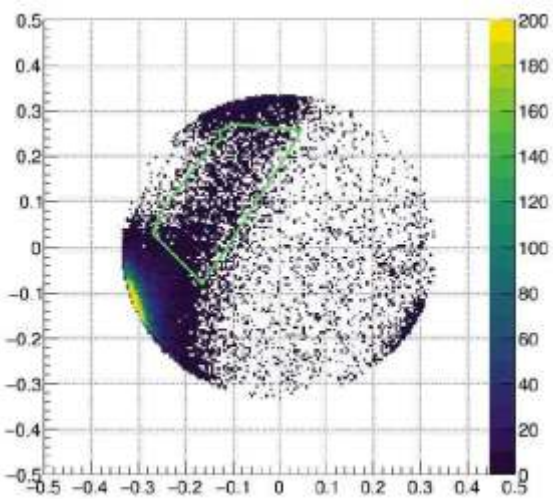

Fig 3: A Dalitz plot showing the sequential (green rectangle) and concerted dissociation of $C_2H_2^{3+}$ under 450 keV Xe^{9+}.

The data analysis for SO_2 molecule was completed using the native frames approach. In the analysis it was assumed that the lifetime of the intermediate precursor SO^{2+} formed in step (I) (see, figure 4 (left)) was much greater than its rotational time. Therefore, any directional correlation of rotation would be lost and a uniform angular distribution would be obtained. Using this technique, we were able to quantify and separate the sequential dissociation events from those of concerted ones. To obtain the lifetime of the molecular ion SO^{2+} formed as an intermediate in the three-body sequential dissociation of SO_2^{3+}, a single exponential to the angular distribution (red dotted rectangle in figure 4 (right)) was fitted to obtain a decay parameter which was directly related to the ratio of the molecular lifetime against dissociation and the rotational time period.

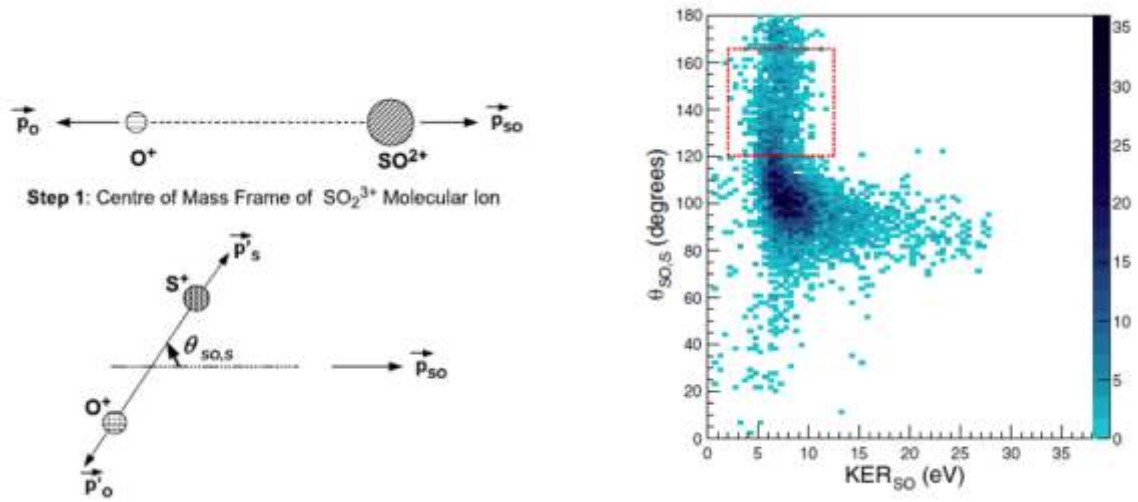

Fig 4: Two steps of the sequential dissociation of SO_2^{3+} formed in the collision of an SO_2 molecule with 450 keV Xe^{9+} (left); Distribution of the kinetic energy release in the unimolecular dissociation of SO^{2+} and $\theta_{SO,S}$ (right). The events within the dotted rectangle were fitted with a single exponential to obtain dissociation lifetime

The analysis of CH_3Cl data was also completed and the yields and the kinetic energy releases (see, figure 5) for the seven dissociation channels of CH_3Cl^{x+} (x=2,3) were obtained. These results were sent to our theoretical collaborators in France who are presently performing the related *ab-initio* calculations.

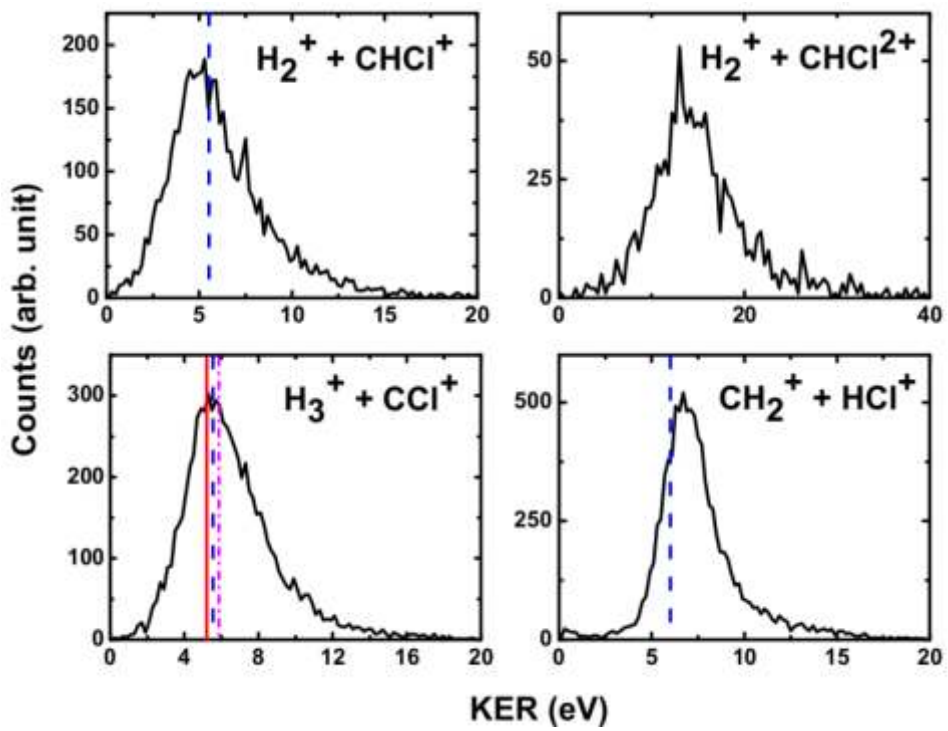

Fig 5: Kinetic energy release distributions for the channels involving bond rearrangement in the dissociation of CH_3Cl^{x+} (x=2,3) under 450 keV Ar^{9+} (black curve); vertical dashed blue and dashed-dotted magenta lines show the experimental KERs reported in the literature under high intensity laser. The solid vertical red line shows the theoretical value of KER reported in the literature.

4.6.4 DEVELOPMENT OF ION TRAP FACILITY AT IUAC

Sugam Kumar[1], C.P. Safvan[1], Pragya Bhatt[1], Deepak Chimmwal[2], Lekha Nair[2], W. Quint[3], M. Vogel[5]

[1]Inter University Accelerator Centre (IUAC), Aruna Asaf Ali Marg, New Delhi, India

[2]Jamia Millia Islamia University, New Delhi, India

[3]GSI Helmholtzzentrum für Schwerionenforschung, Darmstadt, Germany

4.6.4.1 Introduction:

The proposed ion trap facility to be setup at IUAC will be a national user facility, capable of providing a wide range of experimental opportunities to scientists and research students using highly charged ions in the field of atomic and molecular physics.

The construction of the facility is undergoing in two phases. In the first phase, we are constructing compact open endcap cylindrical Penning Trap with a 0.8T permanent magnet as a tool for enabling isolation and manipulation of the charged particles from 10 GHz ECR ion source in a well-controlled environment to study the lifetime of the forbidden metastable transitions in the highly charged atomic and molecular ions. We are proposing to measure the lifetime of the $^2P_{1/2} \rightarrow {}^2P_{3/2}$ transitions in the boron-like ions (S^{11+}, Cl^{12+}, K^{14+}, Ca^{15+}, Sc^{16+} etc.) and lifetime of the $^3P_0 \rightarrow {}^3P_1$ transitions in the Carbon-like ions. (Ca^{14+}, Sc^{15+}, Ti^{16+}, V^{17+}, Cr^{18+} etc.). This will be a user facility in the Low Energy Ion Beam Facility (LEIBF) at the IUAC. Development work of the ion trap for first phase is already started. Schematic of the experimental plan is shown in figure 1.

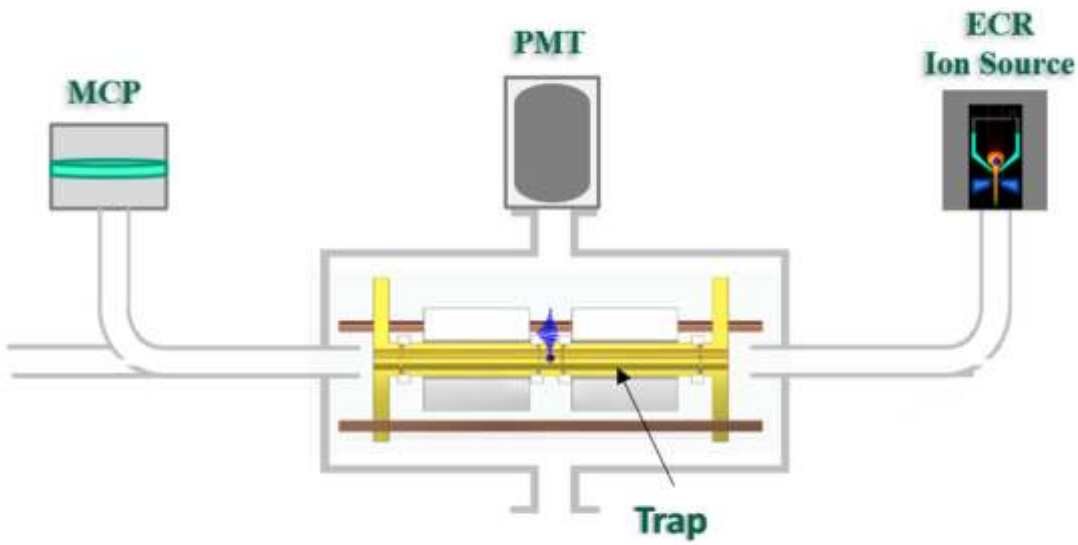

Fig 1. Schematic of the Delhi Penning Trap experimental setup for the measurement of radiative lifetime of the forbidden metastable transitions in the highly charged atomic and molecular ions.

In the second phase, we at IUAC plan to construct an ion trap using a 6T superconducting magnet to produce highly charged ions using a high-energy electron beam from Delhi Light Source (DLS). The proposed experiment has two objectives, the first objective is to measure the *g*-factor of the bound electron in H-like ions with high precision in Penning trap to test the theory of quantum electrodynamics (QED) in an extremely strong electric field of the nucleus. The second objective is to study the evolution of the charge states by successive electron removal by electron impact of kinetic energy in the range of 2-5MeV produced from the DLS as well as to determine the relative cross-section of the successive ionization. The electron impact ionization cross-section at lower electron energies (keV range) has been studied but not in the range of MeV energies. The comparison of the experimental *g*-factors to the theoretically predicted ones will also provide stringent tests of QED calculations.

4.6.4.2 Development of various SUBSYSTEMS OF PHASE-I OF DELHI PENNING TAP (DPT):

The developments in the major areas of the Phase - I of DPT are listed in the following sections:

4.6.4.2.1 The simulation of ion trap

We have designed a Penning Trap customized in a way that external ions can be easily injected into the trap and

stored for the experiment related to lifetime measurement in highly charged atomic or molecular ions. We have done the ion simulation in SIMION to find out the proper electrode size. The optimization of electrode length is done by flying ions and looking at the difference in the trap potential depth obtains after SIMION simulation with the actual harmonic potential at the center of the trap. The electrode potential can be varied to change potential depth to trap ions of different energy in the order of a few hundred electron volts (times the charge state).

The optimized length of the ring electrode is 8.0mm with an inner diameter of 9mm. Since the trap electrodes will fit inside the bore of the permanent magnet and endcap electrode should come out from the bore for better stability. We optimized this length in the SIMION which comes out to be 90mm. The three-pole mechanically compensated trap is attached with additional pair of capture electrodes of length 12mm. The total length of the trap is 234mm. The gap between the ring and endcap electrode is kept at 0.5mm while between the endcap and capture electrode it is 1mm. The electrodes are separated from each other by sapphire rings.

4.6.4.2.2 The CAD design:

The 3D cad drawing of the trap electrode as well as of the whole experimental setup is done using solid edge software. The technical drawings of the trap electrodes were prepared and sent to GSI Workshop for machining. Since the ring electrode will be used for FTICR, therefore the ring electrode is split into 4 segments. A Gap of 0.25mm separation between each segment has been kept.

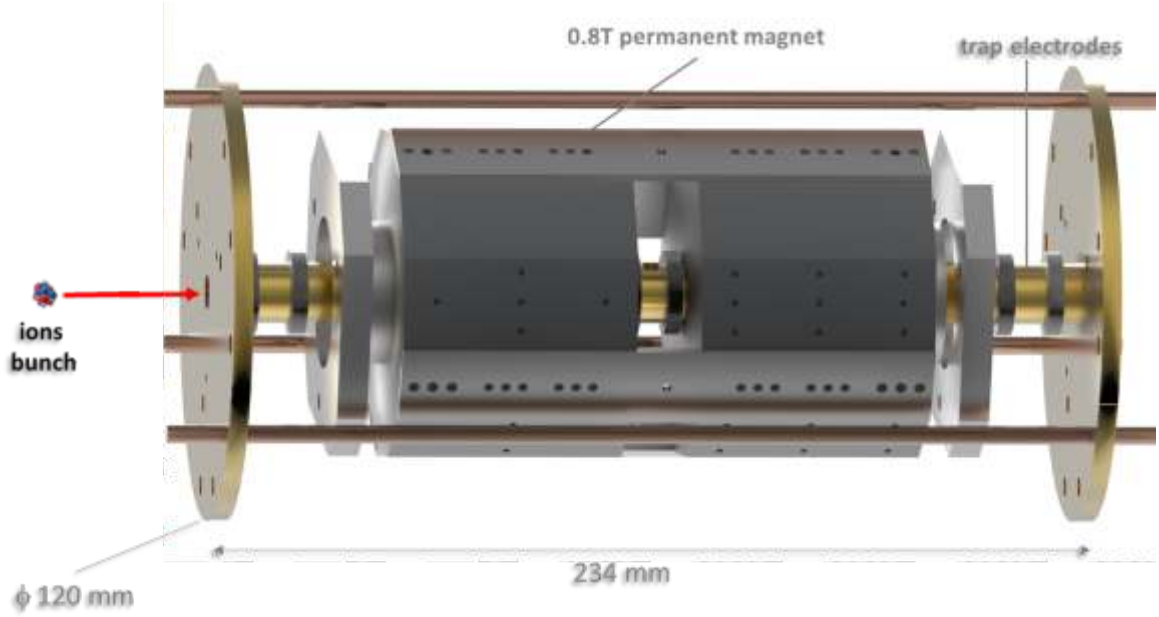

Fig 2. A 3D CAD design of the trap electrode inside the permanent magnet.

Segmented ring electrodes are separated from others with rectangular pieces of sapphire blocks as shown in figure 3. Sapphire has excellent heat conduction properties at best electrical insulation properties, ultra-low dielectric loss tangent, and high mechanical stability. These sapphire blocks maintain the 0.25mm separation between all segments.

One of the end cap electrodes is also segmented into two halves for the purpose of ensuring coupling between different motions and for field excitation. The whole electrodes assembly is sandwiched between two endplates and held together with three copper rods of 5mm diameter in an azimuthal plane at 120^0 separation.

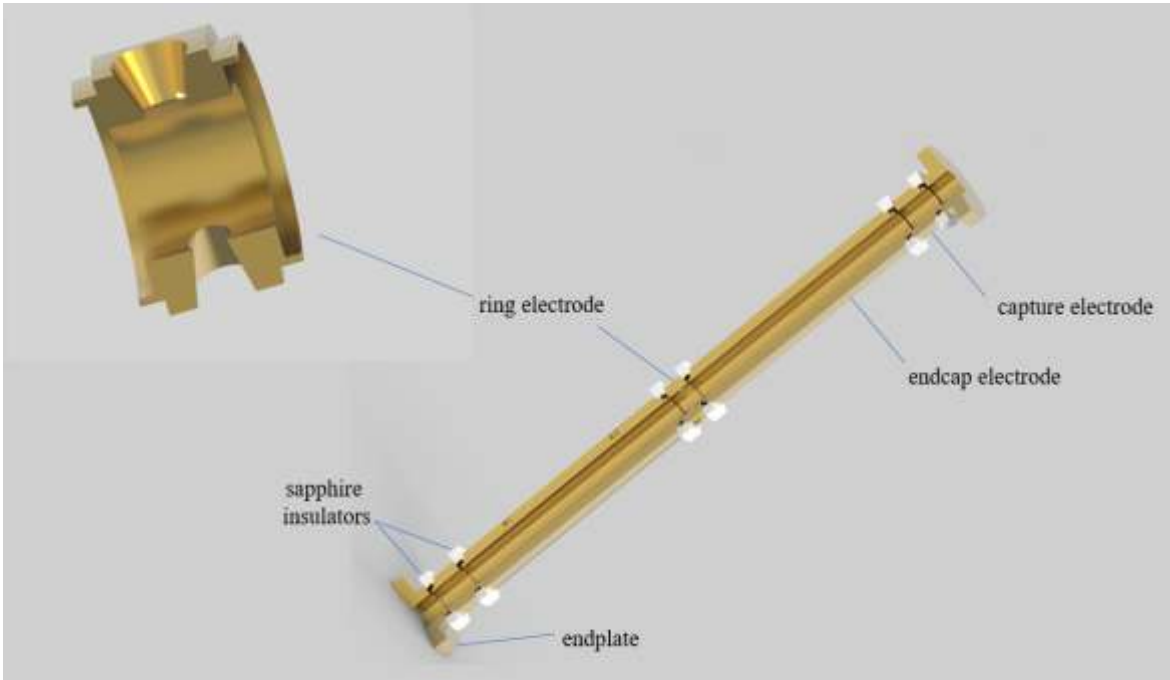

Fig 3. 3D CAD drawing of the trap electrodes. It is consisting of segmented ring electrode with conical hole for the detection of emitted light, two sets of endcap electrodes and capture electrodes. Sapphire insulator isolated electrodes.

4.6.4.2.3 Permanent Magnet

A refurbished permanent magnet has been obtained from GSI, Germany. It is SmCo magnet with remanent field of 1.1 T. Picture of fully assembled permanent magnet is shown in figure 4. The accessible bore diameter of the magnet is 17mm. The whole Penning trap electrodes are inserted inside the magnet bore as shown in figure 2. The whole magnet and trap electrode assembly will be inside the high vacuum chamber.

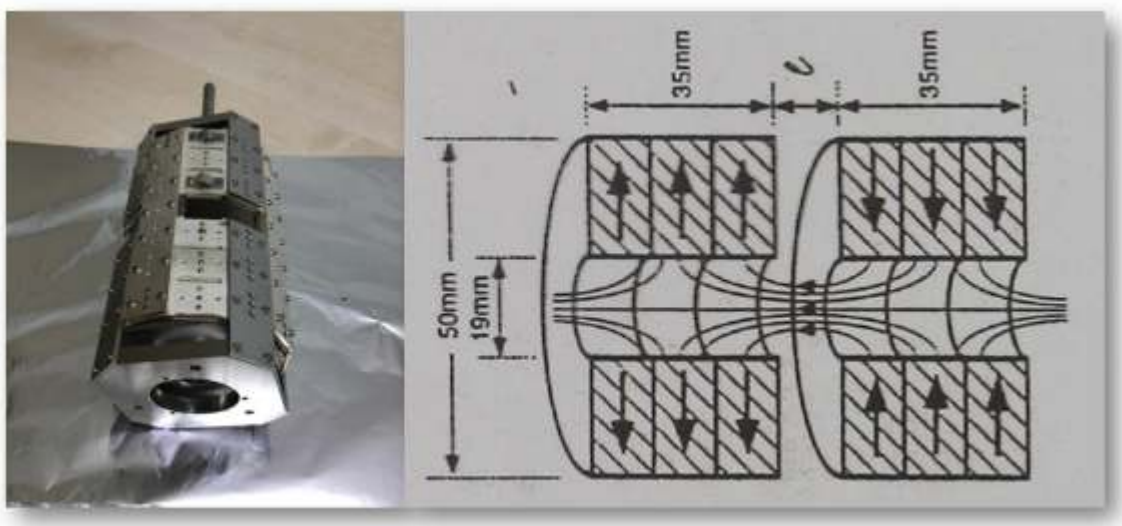

Fig 4. Picture and field alignment of the SmCo permament magnet.

4.6.4.2.4 Manufacturing of the Vacuum Chamber

For mounting ion trap, magnet, the cryo-cooler, extracting signal wires and for pumping, an ultra-high vacuum (UHV) cryo-chamber has been designed and built from 304L stainless steel tubing. The cryo-cooler will be attached to the top CF200 flange port of the cryo-chamber. The penning trap will be connected to the 4K stage (second stage) of the cryo-cooler through long copper through copper-stranded cables. Fourvac technology, Pune manufactured the ultra-high vacuum chamber. The vacuum leak rate has been carried out at IUAC. The ultimate vacuum without proper baking is around $2x10^{-8}$ mbar.

Fig 5. Picture of the ultra-high vacuum chamber during vacuum leak tests.

4.6.4.2.5 Machining of trap electrodes

The trap electrodes are machined in the technical workshop of GSI, Germany. Oxygen-free high-thermal-conductivity (OFHC) copper material has been used to make trap electrodes. The purity of the copper is > 99.999% to minimize the magnetic permeability caused by impurities.

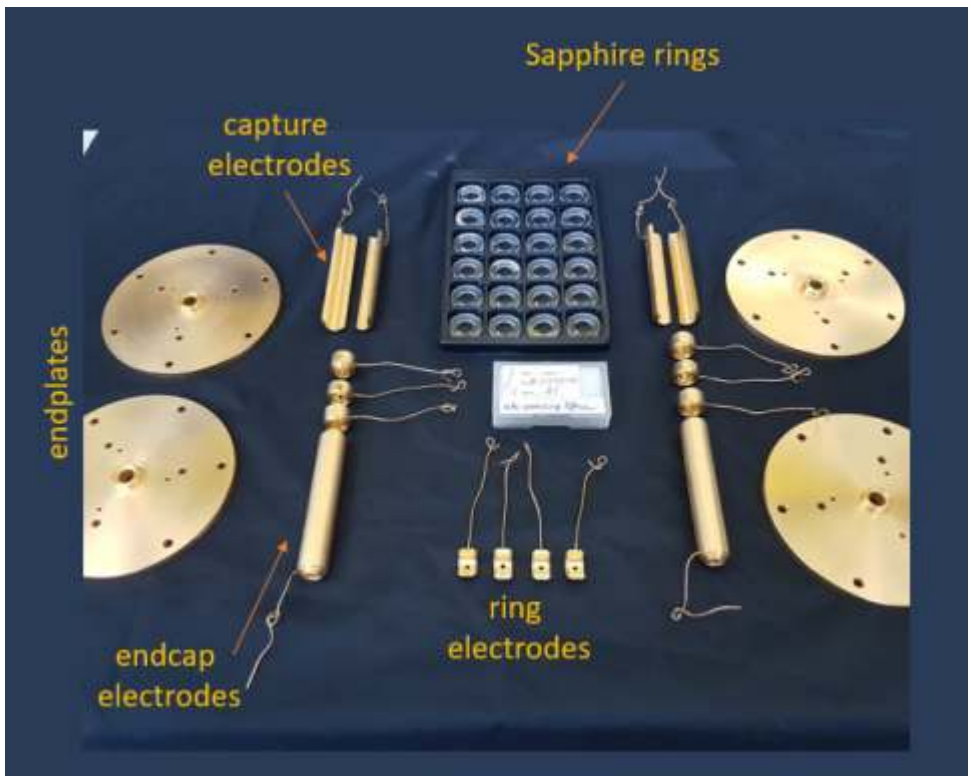

Fig 6. Picture of the precisely machined and gold-plated trap electrodes along with sapphire rings and spacers.

The inner radius and spacing between the electrodes are made within the accuracy of <20μm. To protect the surfaces against oxidation, all OFHC copper electrodes are gold plated electrolytically. The copper surface is first covered with a silver layer to avoid the diffusion of the external gold layer and then the gold of about 1 μm thickness is plated on it, which avoids oxidation and thus a distortion of the electrostatic potential due to charges on the surface. Before the gold plating, the surface was mechanically polished. Two sets of machined trap electrodes acquired form GSI along with sapphire rings and spacers are shown in figure 6.

4.6.4.3 Conclusion

The machined and gold-plated electrodes are already acquired form GSI. We are in process of machining assembly components, as soon it finishes, we will start the assembly of the electrodes and magnet. The whole magnet and trap assembly system will be mounted inside the vacuum chamber. The whole system after assembly will again undergo a vacuum test.

References:

[1] P. J. Mohr, et. al. Newell, Rev. Mod. Phys. 84, 1527 (2012).

[2] C. W. Chou, et. al., Phys. Rev. Lett. 104, 070802 (2010).

[3] G. Gabrielse, Phys. Rev. Lett. 102, 172501 (2009).

[4] R. S. Van Dyck, et. al. Phys. Rev. A 40, 6308 (1989).

[5] Sturm, S.;Wagner, et. al. g-factor of hydrogen-like 28Si13+. Phys. Rev. Lett. 2011, 107, 023002

[6] Sugam Kumar et. al. . Properties of a cylindrical Penning trap with conical endcap openings, Physica Scripta, 90, 075401, 2019